



Published in final edited form as:

Cell Rep. 2018 September 11; 24(11): 2919–2931. doi:10.1016/j.celrep.2018.08.036.

Sarcoplipin Signaling Promotes Mitochondrial Biogenesis and Oxidative Metabolism in Skeletal Muscle

Santosh K. Maurya^{1,3}, Jose L. Herrera¹, Sanjaya K. Sahoo¹, Felipe C.G. Reis¹, Rick B. Vega¹, Daniel P. Kelly², and Muthu Periasamy^{1,4,*}

¹Sanford Burnham Prebys Medical Discovery Institute, Orlando, FL 32827, USA

²Perelman School of Medicine at the University of Pennsylvania, Philadelphia, PA, USA

³Present address: Department of Internal Medicine, The Ohio State University Wexner Medical Center, Columbus, OH 43210, USA

⁴Lead Contact

SUMMARY

The major objective of this study was to understand the molecular basis of how sarcoplipin uncoupling of SERCA regulates muscle oxidative metabolism. Using genetically engineered sarcoplipin (SLN) mouse models and primary muscle cells, we demonstrate that SLN plays a crucial role in mitochondrial biogenesis and oxidative metabolism in muscle. Loss of SLN severely compromised muscle oxidative capacity without affecting fiber-type composition. Mice overexpressing SLN in fast-twitch glycolytic muscle reprogrammed mitochondrial phenotype, increasing fat utilization and protecting against high-fat diet-induced lipotoxicity. We show that SLN affects cytosolic Ca²⁺ transients and activates the Ca²⁺/calmodulin-dependent protein kinase II (CamKII) and PGC1 α axis to increase mitochondrial biogenesis and oxidative metabolism. These studies provide a fundamental framework for understanding the role of sarcoplasmic reticulum (SR)-Ca²⁺ cycling as an important factor in mitochondrial health and muscle metabolism. We propose that SLN can be targeted to enhance energy expenditure in muscle and prevent metabolic disease.

In Brief

Maurya et al. report that sarcoplipin, a regulator of the SERCA pump, promotes mitochondrial biogenesis and oxidative phenotype in muscle. Loss of SLN decreases fat oxidation, whereas

This is an open access article under the CC BY-NC-ND license (<http://creativecommons.org/licenses/by-nc-nd/4.0/>).

*Correspondence: mperiasamy@sbsdsccovery.org.

AUTHOR CONTRIBUTIONS

S.K.M. and M.P. conceived and designed this study. S.K.M. performed all experiments and collected, analyzed, and interpreted the data. J.L.H. and S.K.S. performed and analyzed the Ca²⁺ imaging experiments in myotubes. S.K.M., J.L.H., F.C.R., and M.P. analyzed data. S.K.M. and M.P. wrote the manuscript. D.P.K. and R.B.V. were involved in the design, interpretation of data, and editing of the manuscript

DECLARATION OF INTERESTS

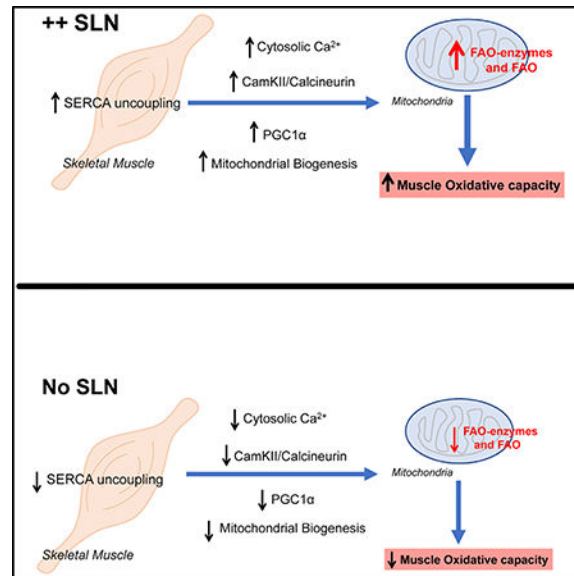
The authors declare no competing interests.

SUPPLEMENTAL INFORMATION

Supplemental Information includes three figures and one table and can be found with this article online at <https://doi.org/10.1016/j.celrep.2018.08.036>.

overexpression of SLN in muscle provides resistance against diet-induced lipotoxicity. By increasing cytosolic Ca^{2+} transients, SLN activates the CamKII-PGC1 α signaling pathway to promote mitochondrial biogenesis.

Graphical Abstract



INTRODUCTION

Skeletal muscle constitutes 40%–50% of body mass in the human adult and is a key determinant of basal metabolic rate and whole-body energy metabolism. Muscle is the major consumer of glucose (nearly 80% of insulin-mediated glucose uptake) and fatty acids (DeFronzo et al., 1981; Thiebaud et al., 1982). It has the ability to increase its energy expenditure 20- to 30-fold during intense exercise by stimulating insulin-independent glucose uptake and by switching to higher fatty acid uptake and oxidation (Lowell and Spiegelman, 2000; Zurlo et al., 1990). Many studies suggest that enhancing energy expenditure in muscle through physical activity could be the most effective strategy for controlling obesity and diabetes, second only to caloric restriction (Gabriel and Zierath, 2017). Apart from physical activity, muscle expends a significant amount of energy to maintain muscle mass through protein synthesis, repair, and regeneration. In addition to contractile function, muscle is the primary organ of heat production in most mammals through shivering and nonshivering thermogenesis, demanding a considerable amount of energy (Arruda et al., 2007; Bal et al., 2012; Block, 1994; Lowell and Spiegelman, 2000; van Marken Lichtenbelt and Daanen, 2003). Data also suggest that muscle can expend energy in the form of heat during diet-induced thermogenesis; however, the mechanisms are not fully understood (Bachman et al., 2002; Bal et al., 2012; Bombardier et al., 2013).

Our laboratory has been exploring the role of sarcoplasmic reticulum (SR)- Ca^{2+} cycling, especially the role of sarcolipin (SLN) and the sarcoendoplasmic reticulum Ca^{2+} ATPase (SERCA) pump in nonshivering thermogenesis (NST). Although SERCA-mediated ATP

hydrolysis is generally coupled to Ca^{2+} transport, we and others have shown that binding of SLN within the SERCA-transmembrane groove promotes uncoupling of SERCA Ca^{2+} transport from ATP hydrolysis; by this mechanism, SLN increases futile SERCA activity, ATP hydrolysis, and thus heat production (Mall et al., 2006; Sahoo et al., 2013, 2015; Smith et al., 2002; Toyoshima et al., 2013; Winther et al., 2013). Using genetically engineered SLN mouse models, we previously reported that SLN plays an important role in muscle thermogenesis and energy metabolism (Bal et al., 2012; Bombardier et al., 2013). Loss of SLN in muscle predisposes mice to develop hypothermia and failure to maintain whole-body temperature during cold exposure. Our studies also revealed that mice lacking SLN were prone to diet-induced obesity, whereas overexpression of SLN in fast and slow twitch fibers led to increased energy expenditure and resistance against high-fat diet-induced obesity (Maurya et al., 2015; Sopariwala et al., 2015). Although these studies implicate SLN as an important regulator of muscle thermogenesis and energy expenditure, the detailed mechanism of how SLN programs and orchestrates oxidative metabolism is not understood. Therefore, in this study, we set out to address the mechanistic basis of SLN signaling both *in vivo* and in primary muscle cells derived from *Sln* knockout (KO) and wild-type (WT) mice. A major objective of this study was to determine the role of SLN in programming mitochondrial phenotype and enhancing fatty acid oxidation in skeletal muscle.

RESULTS

SLN Regulates Mitochondrial Biogenesis and the Switch toward Increased Oxidative Metabolism during Muscle Development

SLN expression is induced severalfold during early neonatal stages of muscle development (in both fast and slow twitch muscle), but its role is not well understood. The neonatal stage is precarious in a newborn's life, with a significant demand for energy to maintain thermogenesis and survive cold. Furthermore, the muscle is undergoing significant growth, differentiation, and maturation due to increased physical activity. To understand the role of SLN in neonatal physiology, we first investigated the relevance of SLN to mitochondrial biogenesis and oxidative metabolism in neonatal muscle of WT and *Sln*-KO mice. SLN expression peaks around birth and continues to be expressed at high levels in all skeletal muscles during the first 10 days of neonatal development (Babu et al., 2007a; Pant et al., 2015, 2016) (Figure 1A). By day 15 postnatally, SLN expression is downregulated in mature glycolytic muscles, including quadriceps, extensor digitorum longus (EDL), and tibialis anterior (TA), but continues to be expressed in oxidative and/or slow twitch muscle, including soleus, red gastrocnemius, and diaphragm (Pant et al., 2015, 2016). This raised the possibility that SLN is important for maintaining the oxidative metabolic phenotype in muscle. Loss of SLN had no effect on muscle fiber size (Figure S1A) and on the expression level of major contractile and SR proteins, including SERCA, calsequestrin 1 and 2 (CASQ1 and CASQ2), muscle α -actin, and α -actinin (Figure 1B).

We next studied how loss of SLN expression affected muscle oxidative capacity in isolated quadriceps muscle from WT and *Sln*-KO mice (10 days old) using high-resolution respirometry. In *Sln*-KO muscle compared to WT, there was a significant decrease in fatty acid (palmitate)-supported oxygen consumption and a significant reduction in succinate-

induced maximal respiration, a sign of reduced fatty acid oxidation (Figure 1C). This is supported by a significant reduction in mtDNA content (Figure 1D) and a drastic reduction in succinate dehydrogenase (SDH) activity in the *Slh*-KO muscle (Figure 1E), indicative of decreased oxidative capacity. Expression of mitochondrial oxidative phosphorylation (OXPHOS) proteins (Figure 1F) and enzymes involved in lipid metabolism, including lipoprotein lipase (LPL), carnitine palmitoyltransferase-1 mitochondrial (CPT1-M), long-chain acyl-coenzyme A (CoA) dehydrogenase (LCAD), hydroxyacyl-CoA dehydrogenase trifunctional multienzyme complex subunit beta (HADHB), citrate synthase, and adenine nucleotide translocator (ANT1/2), in *Slh*-KO muscle compared to WT (Figure 1G). In addition, electron microscopy of *Slh*-KO muscle revealed alteration in mitochondrial morphology, with fewer cristae of smaller length and width (Figures S1B and S1C). However, the expression of genes involved in mitochondrial dynamics, including fusion and fission, was not significantly altered (Figures S1D and S1E). Proteins involved in mitochondrial fusion and fission were higher when normalized to mitochondrial protein VDAC (Figures S1F and S1G). These data suggest that loss of SLN leads to decreased mitochondrial mass but increased mitochondrial dynamics in muscle. We next investigated the autophagy by performing western blotting of LC3 (Figures S1H and S1I) and immunostaining with LC3 and COX4-I1 antibodies (Figures S1J and S1K). The LC3-II/LC3-I ratio, which is an indicator of increased autophagy, is greater in KO muscle (Figures S1H and S1I). Similarly, KO muscle showed higher LC3 staining when normalized with mitochondrial COX4-I1 staining (Figures S1J and S1K).

To our surprise, the 10-day-old *Slh*-KO quadriceps (quads) muscle expressed higher levels of glycolytic enzymes, including phosphofructokinase 1 (PFK1), hexokinase II (HKII), pyruvate kinase muscle (PKM2), and pyruvate dehydrogenase (PDH), which suggest that *Slh*-KO muscle primarily relies on glycolytic metabolism to compensate for decreased fatty acid utilization (Figure 1H). There was an activation of 5' adenosine monophosphate-activated protein (AMP) kinase, alpha (AMPK α) (increased phospho-AMPK α level) in *Slh*-KO quads, indicating a compensatory mechanism to increase energy production (Narkar et al., 2008; Ojuka, 2004) (Figure 1H). These data suggest that SLN is essential for the metabolic switch toward increased fatty acid oxidation in developing muscle. However, quads and gastrocnemius muscle of 10-day-old neonatal *Slh*-KO mice did not show alterations in the expression of myosin isoforms and fiber-type composition (Figures S1L–S1N).

We investigated whether loss of SLN affected oxidative metabolism in soleus muscle of adult mice, which expresses SLN throughout life. In rodents, soleus muscle contains a mixture of both fast oxidative fibers, expressing myosin heavy-chain type IIA (MHC-IIA), and slow twitch fibers, containing the myosin heavy-chain type I (MHC-I) isoform (Rowe et al., 2013), with higher mitochondrial content. Our data show that loss of SLN does not alter mtDNA content in soleus muscle (Figure 1I). Western blot analyses show that the expression level of mitochondrial OXPHOS proteins is not altered in *Slh*-KO soleus compared to WT (Figure 1J); however, there is a reduction in enzymes involved in lipid metabolism (LPL, CPT1-M, LCAD, and HADHB) (Figure 1K) and the ability to oxidize fatty acid (Figure 1L). Enzymes involved in glucose metabolism were not affected (Figure 1M). SDH activity staining confirmed that loss of SLN in soleus muscle decreases its oxidative capacity (Figure

1N). Surprisingly, loss of SLN does not affect the composition of MHC-IIA and MHC-I fibers in soleus muscle (Figure 1O). These data suggest that SLN is critical for maintaining muscle oxidative metabolism, but not fiber-type switching.

SLN Overexpression in Fast Twitch Glycolytic Muscle Reprograms Mitochondria to Increase Fat Oxidation and Resists against Diet-Induced Lipotoxicity

Because SLN expression is downregulated in adult glycolytic muscle, we asked whether transgenic expression of SLN in glycolytic muscle promotes oxidative metabolism using the skeletal muscle-specific SLN overexpression (*Sln^{OE}*) mouse model (Sopariwala et al., 2015). Overexpression of SLN in glycolytic muscle (TA, quads, and gastrocnemius) did not result in fibertype switching, and the numbers of oxidative and glycolytic muscle fibers were similar to those of WT muscle (Figures S2A and S2B). In addition, SLN overexpression did not affect mtDNA content (Figure 2A) or the expression level of OXPHOS proteins in TA muscle (Figure 2B). However, SLN overexpression caused an increase in fatty acid transport proteins, especially CD36, CPT1-M, LPL, and mitochondrial enzymes involved in fatty acid oxidation, like LCAD and HADHB (Figure 2C). Furthermore, glycolytic muscle fibers overexpressing SLN showed higher fatty acid oxidation as measured by oxidation of fatty acid substrates (palmitoylCoA + carnitine) in comparison to *Sln*-KO muscle (Figure 2D). Expression of fusion and fission genes was not significantly different (Figure S1C). However, when expression of fusion and fission proteins was normalized with VDAC protein levels, *Sln^{OE}* muscle showed a lower abundance of mitochondrial dynamic proteins (Figures S2D and S2E).

We next investigated whether higher SLN expression and activity can prevent high-fat diet (HFD)-induced metabolic abnormalities in muscle. HFD feeding induced a significant increase in mtDNA copy number (Figure 2E), the expression of OXPHOS protein complexes (Figure 2F), and enzymes involved in fatty acid metabolism in glycolytic muscle (TA) of *Sln^{OE}* compared to WT muscle (Figure 2G). This increase in mitochondrial metabolic enzymes was supported by a significant increase in fatty acid oxidation (palmitoylcarnitine) in *Sln^{OE}* muscle (Figure 2H). TA muscle of *Sln^{OE}* mice did not show lipid accumulation compared to WT muscle (very low SLN expression) (Figure 2I) and *Sln*-KO muscle (Figure S2F). Conversely, *Sln*-KO soleus showed significant accumulation of lipid droplets compared to WT soleus (high SLN expression) (Figure 2J), a sign of decreased fat utilization, whereas muscle overexpressing SLN did not show signs of lipid accumulation. Furthermore, we observed a lower intramuscular concentration of ceramide, diacylglycerides (DAGs), and acylcarnitines in *Sln^{OE}* muscle compared to WT (Figure 2K). Studies have shown that excess accumulation of these lipid intermediates contributes to lipotoxicity and insulin resistance in skeletal muscle (Samuel and Shulman, 2012; Shulman, 2014; Szendroedi et al., 2014); therefore, we next investigated the muscle glucose uptake and glucose clearance in live mice using hyperinsulinemic-euglycemic clamp (Figure 2L). As expected, *Sln^{OE}* mice displayed a higher rate of muscle glucose uptake and clearance compared to WT mice, suggesting enhanced muscle insulin sensitivity. Conversely, *Sln*-KO mice showed a lower rate of muscle glucose uptake and clearance compared to WT mice, suggesting insulin resistance in *Sln*-KO muscle (Figure S2G). Altogether, these findings strongly suggest that increased SLN expression in muscle reprograms mitochondria,

enhances fatty acid oxidation, and protects against lipotoxicity, thus improving insulin sensitivity.

SLN Recruits PGC1 α to Activate Mitochondrial Biogenesis

To explore the mechanistic details of how SLN regulates mitochondrial phenotype, we took advantage of primary muscle cell cultures derived from *Slm*-KO and WT mice (Figure 3A). SLN is not expressed in myoblast, but its expression is relatively high in differentiating WT myotubes (Figure 3B). Both WT and *Slm*-KO myotubes expressed normal levels of contractile (α -actinin and α -actin) and SR-Ca²⁺ transporter SERCA2 (Figure 3C). However, *Slm*-KO myotubes showed a significant decrease in mitochondrial content, as observed by lower mtDNA copy number (Figure 3D) and decreased expression of OXPHOS protein complexes (Figure 3E). However, the expression of genes involved in mitochondrial dynamics, including fusion and fission, was not significantly altered (Figures S3A and S3B). *Slm*-KO myotubes showed a lower rate of fatty acid oxidation and a decreased oxygen consumption rate (OCR), supporting the lower mitochondrial content (Figures 3F and 3G), whereas the rate of glycolysis and glycolytic capacity (as measured by the extracellular acidification rate [ECAR]) of *Slm*-KO myotubes was higher than that of WT myotubes (Figures S3C and S3D). We next tested whether re-expression of SLN through adenoviral gene transfer could rescue the mitochondrial phenotype in *Slm*-KO myotubes (Figure 3H). Re-expression of SLN in *Slm*-KO myotubes restored mtDNA content (Figure 3I), respiratory capacity (OCR) (Figure 3J), and PGC1 α expression to WT control levels (Figure 3K).

In WT myotubes, PGC1 α expression increased progressively during differentiation (Figure 3L), whereas loss of SLN caused a decrease in the expression level of PGC1 α , PPAR δ , and TFAM (Figures 3L and 3M). PGC1 α is the master regulator of mitochondrial biogenesis, especially in muscle. Therefore, we next addressed whether SLN mediates its effect through upregulation of PGC1 α by using small interfering RNA (siRNA)-mediated knockdown (KD) of PGC1 α in WT and *Slm*-KO primary myotubes. As previously reported, PGC1 α KD in WT myotubes decreased mtDNA copy number, OXPHOS protein expression, and OCR (Figures 3N–3P). We tested whether the rescue of *Slm*-KO myotubes by adenoviral SLN gene transfer is mediated through PGC1 α . We show that knocking down PGC1 α blunted the effect of adenoviral SLN (Ad-SLN) on mitochondrial biogenesis, including mtDNA copy number, OXPHOS protein expression, and OCR (Figures 3N–3P; Figure S3C). Conversely, overexpression of PGC1 α in *Slm*-KO myotubes partially rescued mitochondrial biogenesis compared to WT myotubes (Figure 3Q). These experiments demonstrate that SLN recruits PGC1 α to promote mitochondrial biogenesis.

SLN Alters Cytosolic Ca²⁺ Transients and Activates Ca²⁺-Dependent Signaling Pathways

To determine whether SLN affected cytosolic Ca²⁺ transients, we performed Ca²⁺ imaging using green fluorescent dye (Fluo-4) in C2C12 myotubes expressing high levels of SLN through Ad-SLN gene transfer (Figures 4A–4C). Myotubes expressing SLN showed a higher percentage of cytosolic Ca²⁺ transients (>18%) compared to nontransfected (NT) myotubes in response to caffeine-induced Ca²⁺ release. The Ad-SLN-transfected myotubes show an increase of >2 s in the average time of fluorescence in the cytosol, measured at 50% of the peak; these myotubes also showed a slower decay of the fluorescence in the cytosol,

as measured by the slope (0.088 interval [int]/ms) compared to NT (0.090 int/ms) (Figure 4C). These data indicate a slower Ca^{2+} removal by SERCA in the presence of SLN. However, fluorescence measured 60 s post-stimulation with caffeine showed higher levels of cytosolic Ca^{2+} in Ad-SLN-transfected myotubes (>28%) compared to NT myotubes (Figure 4C). Cytosolic Ca^{2+} remained higher over the course of the experiment in Ad-SLN-transfected myotubes compared to NT control myotubes. These data suggest that SLN shapes cytosolic Ca^{2+} dynamics by increasing the duration of Ca^{2+} transients in the cytosol, which activates Ca^{2+} -dependent signaling mechanisms.

To determine whether SR- Ca^{2+} cycling is a prerequisite for SLN signaling, we manipulated SR- Ca^{2+} release in myotubes using caffeine to sensitize (Darcy et al., 2016) and dantrolene to inhibit RYR1, the primary Ca^{2+} release channel in skeletal muscle SR (Cherednichenko et al., 2008). Treatment with 3.5 mM caffeine resulted in an increase in phosphorylated Ca^{2+} /calmodulin-dependent protein kinase II (pCamKII) activation and Mef2c expression in WT myotubes, but not in *Slh*-KO myotubes (Figure 4D). Caffeine treatment of WT myotubes increased mitochondrial biogenesis, as measured by mtDNA content (Figure 4E), PGC1 α , (Figure 4F), and PPAR δ , TFAM, and metabolic enzymes (Figure 4G), whereas *Slh*-KO myotubes failed to show an increase in mitochondrial biogenesis (Figures 4D–4G). Furthermore, caffeine-treated WT myotubes showed a significant increase in mitochondrial respiration, but *Slh*-KO myotubes showed a poor response to caffeine treatment (Figure 4H). In contrast, inhibition of SR- Ca^{2+} release by dantrolene treatment (10 μM) decreased CamKII activation, mitochondrial biogenesis (Figures 4I–4L), and respiratory capacity only in SLN-expressing myotubes (Figure 4M). We show that inhibition of CamKII activation by pretreatment with KN93 decreased mitochondrial biogenesis and respiratory capacity in WT myotubes. In contrast, SLN re-expression in *Slh*-KO myotubes rescued the phenotype, as evident by increased CamKII activity, mtDNA content, and respiration (Figures 4N–4P). Altogether, these data demonstrate that SLN is essential for the Ca^{2+} -dependent increase in mitochondrial biogenesis and this directly depends on SR- Ca^{2+} cycling and recruitment of the CamKII-PGC1 α axis (Figure 4Q).

DISCUSSION

SLN is an important regulator of the SERCA pump, which is expressed exclusively in striated muscle of all mammals, including humans (Paran et al., 2015; Rowland et al., 2015; Vangheluwe et al., 2005). Studies have shown that SLN binds to SERCA in a Ca^{2+} -sensitive manner and its binding can lead to uncoupling of SERCA pump activity (Sahoo et al., 2013, 2015; Smith et al., 2002). However, the molecular basis of SLN-SERCA interaction is still under intense investigation. Studies have shown that SLN binding to SERCA does not interfere with ATP hydrolysis of the pump but prevents Ca^{2+} transport into the SR lumen, thus promoting slippage of Ca^{2+} back to the cytosol (Mall et al., 2006; Sahoo et al., 2013, 2015). By this mechanism, SLN promotes futile cycling of the pump, increases heat generation, and plays an important role in muscle thermogenesis (Shaikh et al., 2016). Unlike UCP1 in brown adipose tissue (BAT), which dissipates proton gradient (decreasing proton motive force for ATP generation) and generates heat (Betz and Enerbäck, 2018), SLN creates energy demand via futile SERCA activity, increased ATP hydrolysis, and heat production responsible for muscle NST. Using genetically engineered SLN mouse models,

we have shown that SLN is important for adaptive thermogenesis, including cold and diet-induced thermogenesis (Bal et al., 2012). Previously, we reported that an increase in the SLN-toSERCA ratio due to SLN overexpression in muscle can promote increased energy expenditure and provide resistance against diet-induced obesity (Maurya et al., 2015; Sopariwala et al., 2015). In the present study, we investigated the mechanistic basis for the SLN-mediated increase in oxidative metabolism in muscle. We specifically studied how SLN affects mitochondrial phenotype *in vivo* and in primary muscle myotubes. Our studies provide a fundamental framework for the understanding of how regulation of SR-Ca²⁺ cycling can be a powerful signal to regulate mitochondrial oxidative capacity and energy metabolism in muscle.

In this study, we addressed the physiological relevance of high SLN expression during neonatal muscle development in both fast twitch (glycolytic) and slow twitch (oxidative) muscle. Our results point out that SLN is critical for mitochondrial biogenesis and that loss of SLN leads to decreases in mitochondrial content and fatty acid oxidation. In addition, the mitochondria in *Slm*-KO muscle had fewer cristae and expressed lower levels of enzymes involved in fatty acid transport and oxidation. *Slm*-KO muscle shows upregulation of the glycolytic pathway as a compensatory mechanism. These data suggest that SLN plays a critical role in neonatal muscle to orchestrate a metabolic switch toward increased lipid oxidation, a signature of mature muscle mitochondria (Lin et al., 2002; Scarpulla et al., 2012). These and other published data suggest that SLN expression is essential to meet the thermogenic and metabolic demand for survival of the neonates (Nowack et al., 2017; Sepa-Kishi et al., 2017).

Our studies also highlight that a loss of SLN in oxidative and/or slow twitch muscle compromised oxidative capacity and that this is largely due to reduced expression of fatty acid transporters and mitochondrial oxidative enzymes. However, loss of SLN did not affect the fiber-type composition or myosin expression in slow twitch soleus muscle. The most interesting finding of this study was that SLN overexpression in glycolytic muscle induced an oxidative metabolic phenotype by reprogramming mitochondria without affecting the fiber-type composition. The mitochondria of *Slm*^{OE} muscles contained higher levels of fatty acid transporters (CPT1-M) and enzymes involved in beta-oxidation (LCAD/HADHB). In addition, proteins involved in fatty acid import to cytosol (CD36) and lipolysis (LPL) were increased to synchronize increased oxidative metabolism. These results and data from neonatal muscle suggest that SLN is critical for maintaining the oxidative capacity of the muscle.

It has been shown that dysfunction or decrease in muscle oxidative metabolism leads to increased lipid accumulation, causing lipotoxicity and insulin resistance (Aon et al., 2014; Lanza and Nair, 2009). We found that loss of SLN compromised mitochondrial function and its ability to enhance fat oxidation in muscle. When challenged with HFD, the *Slm*-KO muscle showed decreased fatty acid oxidation, increased intramuscular lipid accumulation, and higher concentration of toxic lipid derivatives (ceramide, DAGs, and acylcarnitines). In contrast, overexpression of SLN increased fat oxidation but showed no evidence of intramuscular lipid accumulation and toxic lipid derivatives in glycolytic muscle. The observed lipid accumulation in *Slm*-KO muscle is likely due to decreased energy expenditure

and lower fat oxidizing capacity, whereas SLN overexpression increased energy expenditure and reprogrammed the muscle metabolism to enhance fatty acid oxidation. Several studies have shown that lipotoxicity is tightly linked to muscle insulin resistance and impairment of insulin-mediated glucose uptake (Abdul-Ghani et al., 2008; Bergman et al., 2012; Shulman, 2014). Our data demonstrate that overexpression of SLN improved insulin sensitivity, whereas *Slm*-KO mice showed a sign of insulin resistance. These data collectively suggest that SLN plays a prominent role in regulating muscle oxidative capacity, thereby preventing excess fat accumulation and insulin resistance.

An important objective of this study was to understand the mechanistic basis of how SLN signals to program mitochondrial biogenesis and oxidative metabolism in muscle. Previous studies have shown that SLN affects SR- Ca^{2+} cycling and modifies cytosolic Ca^{2+} during muscle contraction (Sopariwala et al., 2015; Tupling et al., 2011). We show here that SLN interaction with SERCA alters cytosolic Ca^{2+} transients, leading to activation of Ca^{2+} -dependent signaling pathways, especially CamKII, and increased PGC1 α expression. Published studies and results from this study demonstrate that an increase in cytosolic Ca^{2+} transients leads to activation of Ca^{2+} signaling pathways and recruitment of PGC1 α to promote mitochondrial biogenesis (Chin, 2005; Lee et al., 2018; Mansueto et al., 2017; Michel et al., 2007; Wright et al., 2007; Wu et al., 2002). Another key transcription factor, transcription factor EB (TFEB), because of its calcium-dependent regulation, may also be involved in this SLN-dependent signaling pathway (Mansueto et al., 2017). This is especially relevant in light of the decreased TFEB phosphorylation due to increased calcineurin activity in *Slm*^{OE} muscle. In this study, we provide evidence that SR- Ca^{2+} cycling acts as a strong signal to modulate mitochondrial biogenesis. By manipulating SR- Ca^{2+} release with caffeine and dantrolene, we demonstrate that activation of PGC1 α depends on SR- Ca^{2+} cycling and SLN/SERCA interaction. Our data suggest that SLN functions to coordinate energy demand with increased energy production by enhancing mitochondrial function and metabolism through calcium signals. Consistent with this model, our results from mouse models also suggest that a higher SLN-to-SERCA ratio leads to increased mitochondrial biogenesis by creating higher energy demand.

Increasing oxidative metabolism and muscle energetics is an attractive strategy to control obesity and metabolic syndrome. It has been reported that muscle mitochondrial biogenesis can be activated by administering AICAR (an AMPK activator) or GW 1516 (a PPAR δ activator) (Narkar et al., 2008). Although these compounds are effective for increasing mitochondrial biogenesis, they do not create energy demand (Weihrach and Handschin, 2018). Unlike these compounds, SLN-activated mitochondrial biogenesis appears to be a physiological homeostatic response, linking energy demand with energy production. Moreover, by increasing energy demand in muscle through modulation of SERCA activity, SLN acts as an exercise mimetic to increase energy expenditure. In addition, SLN activity can be enhanced by activity (e.g., exercise) and by adaptive thermogenesis in response to cold or caloric excess (MacPherson et al., 2016; Nie et al., 2017; Sepa-Kishi et al., 2017). Most importantly, we have not found adverse effects due to SLN overexpression in muscle. SLN overexpression mice show a higher endurance capacity and improved muscle performance by increasing oxidative capacity (Sopariwala et al., 2015).

In summary, our studies suggest that SLN acts as a dual regulator of muscle metabolism: (1) by promoting futile SERCA pump activity, it creates energy demand, playing a role in muscle thermogenesis, and (2) by altering cytosolic Ca^{2+} , SLN signals to activate mitochondrial biogenesis through CamKII/PGC1 α signaling. Hence, we suggest that SLN effectively functions to integrate increased energy demand with increased mitochondrial ATP production and that manipulation of SR- Ca^{2+} cycling through SLN should be considered a strategy to promote mitochondrial health and whole-body energy metabolism.

EXPERIMENTAL PROCEDURES

Animals

The generation of the *Sln*-KO mouse model (Babu et al., 2007b) and *Sln*^{OE} mouse model (Sopariwala et al., 2015) has been described previously. Animal procedures were approved by the Sanford Burnham Prebys Medical Discovery Institute Animal Care and Use Committee (SBP-IACUC) and conducted in accordance with the Guide for the Care and Use of Laboratory Animals. All animal experiments were performed at the regular housing temperature ($22^{\circ}\text{C} \pm 1^{\circ}\text{C}$).

HFD Studies

Sln^{OE}, *Sln*-KO, and WT mice (8 weeks old, n = 12) were fed a HFD (45% calories from fat) (Research Diet) for 12 weeks.

In Vivo Glucose Uptake Using Hyperinsulinemic-Euglycemic CLAMP

Glucose clamping was done as previously described (Ayala et al., 2007, 2011; Costford et al., 2018).

High-Resolution Respirometry Using Oroboros Oxygraph

Measurement of mitochondrial function (oxygen consumption) in permeabilized (with saponin) muscle fibers was performed at 37°C using Oxygraph 2K (Oroboros, Austria) (Duicu et al., 2012). Mitochondrial respiration in permeabilized (with digitonin) primary myotubes was measured as described earlier (Boyle et al., 2012). Fatty acid-supported mitochondrial respiration was measured following the addition of saturating concentrations of palmitate + malate (2 M) and glutamate (500 mM). Maximal respiration supported by electron flux through complex I was measured with the addition of ADP (500 mM). State 3 respirations (maximal coupled respirations) were achieved by adding saturating concentrations of succinate (500 mM). Steady-state O_2 flux for each respiratory state was determined and normalized to fiberbundle dry weight using Datlab 6 software.

Histology and Electron Microscopy of Muscle Tissues

H&E, oil red O, SDH, and myosin heavy chain (MHC) staining were performed as previously described (Ahn et al., 2016; Gan et al., 2013; Jaspers et al., 2014; Zechner et al., 2010). The fiber typing was done using the antibodies MHC-I (red, BA-D5), MHC-IIA (yellow, 2F7), MHC2x (black, unstained), and MHC2b (green, 10F5) from Developmental Studies Hybridoma Bank (East Iowa City, IA) (Wende et al., 2007). Autophagy marker

LC3A/B antibody (Cell Signaling Technology, 4108) and mitochondrial marker COX4-I1 antibody (R&D Systems, AF5814) were used for co-localization staining in muscle sections. The images were captured using Aperio Scanscope (Leica). For transmission electron microscopy, skeletal muscles were fixed with 1% glutaraldehyde solution. The muscle samples were cut and processed as described in Bal et al. (2016) and Zechner et al. (2010). Electron micrographs were obtained using a Tecnai G2 Spirit transmission electron microscope (FEI, Hillsboro, OR). ImageJ (NIH) was used to quantify images.

Quantification of mtDNA Copy Number

The levels of NADH dehydrogenase subunit 1 (Nd1, mtDNA) were quantified (using qPCR) and normalized to the levels of LPL (genomic DNA) (Liang et al., 2016). The primers were mtDNA Nd1 (mt-Nd1) forward (Fw), 5'-CCCATTCGC GTTATTCTT-3'; mt-Nd1 reverse (Rv), 5'-AAGTTGATCG TAACGGAAGC-3'; LPL Fw, 5'-GGATGGACGGTA AGAGTGATTC-3'; and LPL Rv, 5'-ATCCAAGGGTAGCAGACAGGT-3'.

Gene Expression Analysis

Total RNA was isolated from the myotubes using the TRIzol reagent in accordance with the manufacturer's guidelines. 1 µg of RNA was reverse transcribed using the Maxima first strand cDNA synthesis kit (QIAGEN). Gene expression analysis was performed on Roche Real-Time PCR System using custom-designed primers. The list of primers is provided in Table S1.

Lipidomics

Multidimensional mass spectrometry-based shotgun lipidomics methodology was used to measure and characterize the lipid species (ceramides, DAGs, and acylcarnitines) in skeletal muscle. The lipids were extracted from muscle by a modified Bligh and Dyer procedure and measured as previously described (Wang and Han, 2014; Wang et al., 2014).

Primary Muscle Cell Culture

Primary muscle cells were isolated from skeletal muscles as previously described (Gan et al., 2011). For differentiation, cells were washed with PBS, refed with 2% horse serum/DMEM differentiation medium, and then refed daily. Primary myoblasts were infected with an adenovirus overexpressing GFP, SLN, GFP short hairpin RNA (shRNA), or PGC1 α shRNA as previously described (Gan et al., 2013; Kleiner et al., 2009). Twelve hours after infection, cells were differentiated by switching to differentiation medium. Differentiated myotubes were treated with caffeine (3.5 mM), dantrolene (10 µM), or KN93 (1 µM) for 48 hr.

Live-Cell Ca²⁺ Imaging

For confocal imaging of Ca²⁺ dynamics, C2C12 cells were seeded on glass-bottom dishes (MatTek). After 3 days of differentiation, myotubes were infected with adenovirus-containing SLN gene in differentiation medium (DM) for 4 hr. SLN-transfected and NT myotubes were washed with Krebs-Ringer-HEPES (KRH) buffer (125 mM NaCl, 5 mM KCl, 1.2 mM KH₂PO₄, 6 mM glucose, 1.2 mM MgCl₂, 25 mM HEPES) and loaded with

Fluo-4 acetoxymethyl (AM) (5 μ M; Invitrogen, F14201) for 45 min, followed by washes and incubation with KRH for 30 min. For the evaluation of Ca^{2+} cycling in myotubes, fluorescence intensity was monitored by time-lapse microscopy at 60 fps for up to 3 min after the addition of 10 mM caffeine (final concentration, 500 μ M), using a laser confocal microscope with a resonant scanner (Nikon A1R, Nikon Instruments, Melville, NY). Before any stimulation, basal Fluo-4 fluorescence was imaged with a Galvano scanner to study resting calcium levels. Processing and analysis of the acquired images were carried out using Nikon NIS-Elements AR Analysis 4.40 software. Cytosolic Ca^{2+} oscillations were measured at 50% of the peak fluorescence using the time measurement tool in selected multi-regions of interest (multi-ROIs). The SR- Ca^{2+} uptake rate was measured by analyzing the curve slope at 50% of the peak (variation of fluorescence intensity over time). Quantitative analysis was done under a 20 \times objective lens, and approximately 35–45 cells were scored for each experimental condition in five separate analyses ($n = 5$).

OCR and ECAR Using a Seahorse Flux Analyzer

The mitochondrial OCR and ECAR were measured as a function of mitochondrial respiration using a Seahorse XF96 Extracellular Flux Analyzer (Seahorse Bioscience). Before assay, the myotubes were washed and incubated with DMEM without bicarbonate in a CO_2 -free incubator for 1 hr at 37 $^\circ\text{C}$. For OCR measurements, oligomycin (5 mg/mL), carbonyl cyanide-4-(trifluoromethoxy)phenylhydrazone (FCCP) (5 mM), and rotenone (1 mM) were successively injected in the cell assay plate. For ECAR measurement, glucose (10 μ M), oligomycin (1.0 μ M), and 2-Deoxy-glucose (2-DG) (50 mM) were successively injected in the cell assay plate. OCR and ECAR were automatically calculated and recorded by the Seahorse XF96 software Wave.

Western Blotting

Expression levels of mitochondrial and other signaling proteins were determined by western blotting as previously described (Kanzleiter et al., 2014). Skeletal muscle tissues were homogenized in ice-cold homogenization buffer (137 mM NaCl, 2.7 mM KCl, 1 mM MgCl_2 , 5 mM $\text{Na}_4\text{O}_7\text{P}_2$, 10 mM NaF, 100% nonidet P-40, 10% glycerol, 20 mM Tris [pH 7.8], 1 mM EDTA, 0.2 mM PMSF, 0.5 mM Na_3VO_4 , protease inhibitor cocktail). After electrophoresis, proteins were transferred to 0.2 or 0.45 μ m nitrocellulose membranes. Membranes were blocked for nonspecific binding at room temperature (RT) for 1 hr using LI-COR blocking buffer + tris buffered saline (TBS)-Tween 20 (TBS-T) (1:1 v/v). Membranes were probed with primary antibodies for either 2 hr at RT or overnight at 4 $^\circ\text{C}$. The following primary antibodies were used: SLN (Millipore, ABT13), α -actin (Abcam, ab28052), SERCA1a and SERCA2b (custommade antibodies, YenZym, San Francisco), CASQ1 (Fisher, MA3913), CASQ2 (Santa Cruz, sc390999), α -actinin (Sigma-Aldrich, A7811), mitoOXPHOS antibody cocktail (Abcam, ab110413), LPL (Abcam, ab21356), CPT1-M (Alpha Diagnostics, CPT1M11-S), LCAD (Abcam, ab128566), HADHB (Novus Biologicals, NBP1–82609), ANT1/2 (Santa Cruz, sc-9300), citrate synthase (Santa Cruz, sc-390693), HKII (Millipore, AB3279), PFK1 (Santa Cruz, sc67028), GAPDH (Santa Cruz, sc-25778), PKM2 (Santa Cruz, sc-292640), PDH (Cell Signaling Technology [CST], 2784), pAMPK (CST, 2535), AMPK (CST, 5831), CD36 (Santa Cruz, sc-9154), TFAM (Santa Cruz, sc-23588), PGC1 α (CST, 2178), PPAR δ (Abcam, ab137724), p-CamKII alpha (Santa

Cruz, sc12886), CamKII alpha (Santa Cruz, sc-13141), and Mef2c (Abcam, ab70961). After being washed with 0.05% TBS-T, blots were probed with the appropriate infrared (IR)-linked secondary antibody (IRDye, LI-COR) for 1 hr at RT and then washed again with 0.05% TBS-T. Finally, membranes were scanned using a LI-COR Odyssey scanner.

Data Analysis

Statistical analyses were performed using GraphPad Prism software (v.6.0). All data are expressed as means \pm SEM. Where appropriate, a Student's t test or an ANOVA followed by a Tukey or Bonferroni post hoc test was performed. The following levels of significance were used: * $p = 0.01$, ** $p = 0.001$, and *** $p = 0.0001$.

Supplementary Material

Refer to Web version on PubMed Central for supplementary material.

ACKNOWLEDGMENTS

This work was supported, in part, by NIH grant R01 DK098240-01 and by American Diabetes Association Basic Science Research Award (7-13-BS-131) to M.P. NIH grant R01 HL 058493 to D.P.K. is acknowledged. We thank the SBP Medical Discovery Institute's Cardiometabolic Phenotyping Core for *in vivo* glucose uptake studies and John Shelly for histological staining and electron microscopy. We thank Dr Xianlin Han's lab for isolation and quantification of intramuscular lipids species. Technical help from Andrea Bergano and administrative support by Lorenzo Thomas are also acknowledged.

REFERENCES

- Abdul-Ghani MA, Muller FL, Liu Y, Chavez AO, Balas B, Zuo P, Chang Z, Tripathy D, Jani R, Molina-Carrion M, et al. (2008). Deleterious action of FA metabolites on ATP synthesis: possible link between lipotoxicity, mitochondrial dysfunction, and insulin resistance. *Am. J. Physiol. Endocrinol. Metab* 295, E678–E685. [PubMed: 18593850]
- Ahn B, Soundarapandian MM, Sessions H, Peddibhotla S, Roth GP, Li JL, Sugarman E, Koo A, Malany S, Wang M, et al. (2016). MondoA coordinately regulates skeletal myocyte lipid homeostasis and insulin signaling. *J. Clin. Invest* 126, 3567–3579. [PubMed: 27500491]
- Aon MA, Bhatt N, and Cortassa SC (2014). Mitochondrial and cellular mechanisms for managing lipid excess. *Front. Physiol* 5, 282. [PubMed: 25132820]
- Arruda AP, Nigro M, Oliveira GM, and de Meis L (2007). Thermogenic activity of Ca²⁺-ATPase from skeletal muscle heavy sarcoplasmic reticulum: the role of ryanodine Ca²⁺ channel. *Biochim. Biophys. Acta* 1768, 1498–1505. [PubMed: 17466935]
- Ayala JE, Bracy DP, Julien BM, Rottman JN, Fueger PT, and Wasserman DH (2007). Chronic treatment with sildenafil improves energy balance and insulin action in high fat-fed conscious mice. *Diabetes* 56, 1025–1033. [PubMed: 17229936]
- Ayala JE, Bracy DP, Malabanan C, James FD, Ansari T, Fueger PT, McGuinness OP, and Wasserman DH (2011). Hyperinsulinemic-euglycemic clamps in conscious, unrestrained mice. *J. Vis. Exp* 57, 3188.
- Babu GJ, Bhupathy P, Carnes CA, Billman GE, and Periasamy M (2007a). Differential expression of sarcolipin protein during muscle development and cardiac pathophysiology. *J. Mol. Cell. Cardiol* 43, 215–222. [PubMed: 17561107]
- Babu GJ, Bhupathy P, Timofeyev V, Petrashevskaya NN, Reiser PJ, Chiamvimonvat N, and Periasamy M (2007b). Ablation of sarcolipin enhances sarcoplasmic reticulum calcium transport and atrial contractility. *Proc. Natl. Acad. Sci. USA* 104, 17867–17872. [PubMed: 17971438]

- Bachman ES, Dhillon H, Zhang CY, Cinti S, Bianco AC, Kobilka BK, and Lowell BB (2002). BetaAR signaling required for diet-induced thermogenesis and obesity resistance. *Science* 297, 843–845. [PubMed: 12161655]
- Bal NC, Maurya SK, Sopariwala DH, Sahoo SK, Gupta SC, Shaikh SA, Pant M, Rowland LA, Bombardier E, Goonasekera SA, et al. (2012). Sarcolipin is a newly identified regulator of muscle-based thermogenesis in mammals. *Nat. Med* 18, 1575–1579. [PubMed: 22961106]
- Bal NC, Maurya SK, Singh S, Wehrens XH, and Periasamy M (2016). Increased reliance on muscle-based thermogenesis upon acute minimization of brown adipose tissue function. *J. Biol. Chem* 291, 17247–17257. [PubMed: 27298322]
- Bergman BC, Hunerdosse DM, Kerege A, Playdon MC, and Perreault L (2012). Localisation and composition of skeletal muscle diacylglycerol predicts insulin resistance in humans. *Diabetologia* 55, 1140–1150. [PubMed: 22252470]
- Betz MJ, and Enerbäck S (2018). Targeting thermogenesis in brown fat and muscle to treat obesity and metabolic disease. *Nat. Rev. Endocrinol* 14, 77–87. [PubMed: 29052591]
- Block BA (1994). Thermogenesis in muscle. *Annu. Rev. Physiol* 56, 535–577. [PubMed: 8010751]
- Bombardier E, Smith IC, Gamu D, Fajardo VA, Vigna C, Sayer RA, Gupta SC, Bal NC, Periasamy M, and Tupling AR (2013). Sarcolipin trumps b-adrenergic receptor signaling as the favored mechanism for muscle-based diet-induced thermogenesis. *FASEB J.* 27, 3871–3878. [PubMed: 23752204]
- Boyle KE, Zheng D, Anderson EJ, Neuffer PD, and Houmard JA (2012). Mitochondrial lipid oxidation is impaired in cultured myotubes from obese humans. *Int. J. Obes* 36, 1025–1031.
- Cherednichenko G, Ward CW, Feng W, Cabrales E, Michaelson L, Samsó M, López JR, Allen PD, and Pessah IN (2008). Enhanced excitation-coupled calcium entry in myotubes expressing malignant hyperthermia mutation R163C is attenuated by dantrolene. *Mol. Pharmacol* 73, 1203–1212. [PubMed: 18171728]
- Chin ER (2005). Role of Ca²⁺/calmodulin-dependent kinases in skeletal muscle plasticity. *J. Appl. Physiol* 99, 414–423. [PubMed: 16020436]
- Costford SR, Brouwers B, Hopf ME, Sparks LM, Dispagna M, Gomes AP, Cornell HH, Petucci C, Phelan P, Xie H, et al. (2018). Skeletal muscle overexpression of nicotinamide phosphoribosyl transferase in mice coupled with voluntary exercise augments exercise endurance. *Mol. Metab* 7, 1–11. [PubMed: 29146412]
- Darcy YL, Diaz-Sylvester PL, and Copello JA (2016). K201 (JTV519) is a Ca²⁺-dependent blocker of SERCA and a partial agonist of ryanodine receptors in striated muscle. *Mol. Pharmacol* 90, 106–115. [PubMed: 27235390]
- DeFronzo RA, Jacot E, Jequier E, Maeder E, Wahren J, and Felber JP (1981). The effect of insulin on the disposal of intravenous glucose. Results from indirect calorimetry and hepatic and femoral venous catheterization. *Diabetes* 30, 1000–1007. [PubMed: 7030826]
- Duicu O, Gheorghesou D, Mirica N, Trancot S, Cristina D, Fir -Mladinescu O, and Muntean D (2012). High-resolution respirometry with multiple substrates titration in permeabilized myocardial fibers. *Rev. Med. Chir. Soc. Med. Nat. Iasi* 116, 207–213. [PubMed: 23077897]
- Gabriel BM, and Zierath JR (2017). The limits of exercise physiology: from performance to health. *Cell Metab* 25, 1000–1011. [PubMed: 28467920]
- Gan Z, Burkart-Hartman EM, Han DH, Finck B, Leone TC, Smith EY, Ayala JE, Holloszy J, and Kelly DP (2011). The nuclear receptor PPAR β/δ programs muscle glucose metabolism in cooperation with AMPK and MEF2. *Genes Dev.* 25, 2619–2630. [PubMed: 22135324]
- Gan Z, Rumsey J, Hazen BC, Lai L, Leone TC, Vega RB, Xie H, Conley KE, Auwerx J, Smith SR, et al. (2013). Nuclear receptor/microRNA circuitry links muscle fiber type to energy metabolism. *J. Clin. Invest* 123, 2564–2575. [PubMed: 23676496]
- Jaspers RT, Testerink J, Della Gaspera B, Chanoine C, Bagowski CP, and van der Laarse WJ (2014). Increased oxidative metabolism and myoglobin expression in zebrafish muscle during chronic hypoxia. *Biol. Open* 3, 718–727. [PubMed: 25063194]
- Kanzleiter T, Rath M, Penkov D, Puchkov D, Schulz N, Blasi F, and Schürmann A (2014). Pknox1/Prep1 regulates mitochondrial oxidative phosphorylation components in skeletal muscle. *Mol. Cell. Biol* 34, 290–298. [PubMed: 24216763]

- Kleiner S, Nguyen-Tran V, Baré O, Huang X, Spiegelman B, and Wu Z (2009). PPARdelta agonism activates fatty acid oxidation via PGC-1alpha but does not increase mitochondrial gene expression and function. *J. Biol. Chem* 284, 18624–18633. [PubMed: 19435887]
- Lanza IR, and Nair KS (2009). Muscle mitochondrial changes with aging and exercise. *Am. J. Clin. Nutr* 89, 467S–471S. [PubMed: 19056588]
- Lee SH, Hadipour-Lakmehsari S, Miyake T, and Gramolini AO (2018). Three-dimensional imaging reveals endo(sarco)plasmic reticulum-containing invaginations within the nucleoplasm of muscle. *Am. J. Physiol. Cell Physiol* 314, C257–C267. [PubMed: 29167149]
- Liang X, Liu L, Fu T, Zhou Q, Zhou D, Xiao L, Liu J, Kong Y, Xie H, Yi F, et al. (2016). Exercise inducible lactate dehydrogenase B regulates mitochondrial function in skeletal muscle. *J. Biol. Chem* 291, 25306–25318. [PubMed: 27738103]
- Lin J, Wu H, Tarr PT, Zhang C Y, Wu Z, Boss O, Michael LF, Puigserver P, Isotani E, Olson EN, et al. (2002). Transcriptional co-activator PGC-1 alpha drives the formation of slow-twitch muscle fibres. *Nature* 418, 797–801. [PubMed: 12181572]
- Lowell BB, and Spiegelman BM (2000). Towards a molecular understanding of adaptive thermogenesis. *Nature* 404, 652–660. [PubMed: 10766252]
- MacPherson RE, Gamu D, Frendo-Cumbo S, Castellani L, Kwon F, Tupling AR, and Wright DC (2016). Sarcolipin knockout mice fed a high-fat diet exhibit altered indices of adipose tissue inflammation and remodeling. *Obesity (Silver Spring)* 24, 1499–1505. [PubMed: 27345961]
- Mall S, Broadbridge R, Harrison SL, Gore MG, Lee AG, and East JM (2006). The presence of sarcolipin results in increased heat production by Ca(2+)-ATPase. *J. Biol. Chem* 281, 36597–36602. [PubMed: 17018526]
- Mansueto G, Armani A, Viscomi C, D’Orsi L, De Cegli R, Polishchuk EV, Lamperti C, Di Meo I, Romanello V, Marchet S, et al. (2017). Transcription factor EB controls metabolic flexibility during exercise. *Cell Metab.* 25, 182–196. [PubMed: 28011087]
- Maurya SK, Bal NC, Sopariwala DH, Pant M, Rowland LA, Shaikh SA, and Periasamy M (2015). Sarcolipin is a key determinant of the basal metabolic rate, and its overexpression enhances energy expenditure and resistance against diet-induced obesity. *J. Biol. Chem* 290, 10840–10849. [PubMed: 25713078]
- Michel RN, Chin ER, Chakkalakal JV, Eibl JK, and Jasmin BJ (2007). Ca²⁺/calmodulin-based signalling in the regulation of the muscle fibre phenotype and its therapeutic potential via modulation of utrophin A and myostatin expression. *Appl Physiol Nutr Metab.* 32, 921–929. [PubMed: 18059617]
- Narkar VA, Downes M, Yu RT, Emblar E, Wang YX, Banayo E, Mihaylova MM, Nelson MC, Zou Y, Juguilon H, et al. (2008). AMPK and PPARdelta agonists are exercise mimetics. *Cell* 134, 405–415. [PubMed: 18674809]
- Nie L, Yuan XL, Jiang KT, Jiang YH, Yuan J, Luo L, Cui SW, and Sun C (2017). Salsalate activates skeletal muscle thermogenesis and protects mice from high-fat diet induced metabolic dysfunction. *EBioMedicine* 23, 136–145. [PubMed: 28801239]
- Nowack J, Giroud S, Arnold W, and Ruf T (2017). Muscle non-shivering thermogenesis and its role in the evolution of endothermy. *Front. Physiol* 8, 889. [PubMed: 29170642]
- Ojuka EO (2004). Role of calcium and AMP kinase in the regulation of mitochondrial biogenesis and GLUT4 levels in muscle. *Proc. Nutr. Soc* 63, 275–278. [PubMed: 15294043]
- Pant M, Bal NC, and Periasamy M (2015). Cold adaptation overrides developmental regulation of sarcolipin expression in mice skeletal muscle: SOS for muscle-based thermogenesis? *J Exp Biol.* 218, 2321–2325. [PubMed: 26026037]
- Pant M, Bal NC, and Periasamy M (2016). Sarcolipin: a key thermogenic and metabolic regulator in skeletal muscle. *Trends Endocrinol Metab.* 27, 881–892. [PubMed: 27637585]
- Paran CW, Verkerke AR, Heden TD, Park S, Zou K, Lawson HA, Song H, Turk J, Houmard JA, and Funai K (2015). Reduced efficiency of sarcolipin-dependent respiration in myocytes from humans with severe obesity. *Obesity (Silver Spring)* 23, 1440–1449. [PubMed: 25970801]
- Rowe GC, Patten IS, Zsengeller ZK, El-Khoury R, Okutsu M, Bampoh S, Koullis N, Farrell C, Hirshman MF, Yan Z, et al. (2013). Disconnecting mitochondrial content from respiratory chain capacity in PGC-1-deficient skeletal muscle. *Cell Rep.* 3, 1449–1456. [PubMed: 23707060]

- Rowland LA, Bal NC, and Periasamy M (2015). The role of skeletal muscle-based thermogenic mechanisms in vertebrate endothermy. *Biol. Rev. Camb. Philos. Soc* 90, 1279–1297. [PubMed: 25424279]
- Sahoo SK, Shaikh SA, Sopariwala DH, Bal NC, and Periasamy M (2013). Sarcolipin protein interaction with sarco(endo)plasmic reticulum Ca²⁺ ATPase (SERCA) is distinct from phospholamban protein, and only sarcolipin can promote uncoupling of the SERCA pump. *J. Biol. Chem* 288, 6881–6889. [PubMed: 23341466]
- Sahoo SK, Shaikh SA, Sopariwala DH, Bal NC, Bruhn DS, Kopec W, Khandelia H, and Periasamy M (2015). The N terminus of sarcolipin plays an important role in uncoupling sarco-endoplasmic reticulum Ca²⁺-ATPase (SERCA) ATP hydrolysis from Ca²⁺ transport. *J. Biol. Chem* 290, 14057–14067. [PubMed: 25882845]
- Samuel VT, and Shulman GI (2012). Mechanisms for insulin resistance: common threads and missing links. *Cell* 148, 852–871. [PubMed: 22385956]
- Scarpulla RC, Vega RB, and Kelly DP (2012). Transcriptional integration of mitochondrial biogenesis. *Trends Endocrinol. Metab* 23, 459–466. [PubMed: 22817841]
- Sepa-Kishi DM, Sotoudeh-Nia Y, Iqbal A, Bikopoulos G, and Ceddia RB (2017). Cold acclimation causes fiber type-specific responses in glucose and fat metabolism in rat skeletal muscles. *Sci. Rep* 7, 15430. [PubMed: 29133865]
- Shaikh SA, Sahoo SK, and Periasamy M (2016). Phospholamban and sarcolipin: are they functionally redundant or distinct regulators of the sarco(endo) plasmic reticulum calcium ATPase? *J. Mol. Cell. Cardiol* 91, 81–91. [PubMed: 26743715]
- Shulman GI (2014). Ectopic fat in insulin resistance, dyslipidemia, and cardiometabolic disease. *N. Engl. J. Med* 371, 1131–1141. [PubMed: 25229917]
- Smith WS, Broadbridge R, East JM, and Lee AG (2002). Sarcolipin un-couples hydrolysis of ATP from accumulation of Ca²⁺ by the Ca²⁺-ATPase of skeletal-muscle sarcoplasmic reticulum. *Biochem. J* 361, 277–286. [PubMed: 11772399]
- Sopariwala DH, Pant M, Shaikh SA, Goonasekera SA, Molkenkin JD, Weisleder N, Ma J, Pan Z, and Periasamy M (2015). Sarcolipin overexpression improves muscle energetics and reduces fatigue. *J. Appl. Physiol* 118, 1050–1058. [PubMed: 25701006]
- Szendroedi J, Yoshimura T, Phielix E, Koliaki C, Marcucci M, Zhang D, Jelenik T, Müller J, Herder C, Nowotny P, et al. (2014). Role of diacylglycerol activation of PKC ζ in lipid-induced muscle insulin resistance in humans. *Proc. Natl. Acad. Sci. USA* 111, 9597–9602. [PubMed: 24979806]
- Thiebaud D, Jacot E, DeFronzo RA, Maeder E, Jequier E, and Felber JP (1982). The effect of graded doses of insulin on total glucose uptake, glucose oxidation, and glucose storage in man. *Diabetes* 31, 957–963. [PubMed: 6757014]
- Toyoshima C, Iwasawa S, Ogawa H, Hirata A, Tsueda J, and Inesi G (2013). Crystal structures of the calcium pump and sarcolipin in the Mg²⁺-bound E1 state. *Nature* 495, 260–264. [PubMed: 23455422]
- Tupling AR, Bombardier E, Gupta SC, Hussain D, Vigna C, Bloemberg D, Quadrilatero J, Trivieri MG, Babu GJ, Backx PH, et al. (2011). Enhanced Ca²⁺ transport and muscle relaxation in skeletal muscle from sarcolipin-null mice. *Am. J. Physiol. Cell Physiol* 301, C841–C849. [PubMed: 21697544]
- van Marken Lichtenbelt WD, and Daanen HA (2003). Cold-induced metabolism. *Curr. Opin. Clin. Nutr. Metab. Care* 6, 469–475. [PubMed: 12806223]
- Vangheluwe P, Schuermans M, Zádor E, Waelkens E, Raeymaekers L, and Wuytack F (2005). Sarcolipin and phospholamban mRNA and protein expression in cardiac and skeletal muscle of different species. *Biochem. J* 389, 151–159. [PubMed: 15801907]
- Wang M, and Han X (2014). Multidimensional mass spectrometry-based shotgun lipidomics. *Methods Mol. Biol* 1198, 203–220. [PubMed: 25270931]
- Wang M, Hayakawa J, Yang K, and Han X (2014). Characterization and quantification of diacylglycerol species in biological extracts after one-step derivatization: a shotgun lipidomics approach. *Anal. Chem* 86, 2146–2155. [PubMed: 24432906]
- Weihrauch M, and Handschin C (2018). Pharmacological targeting of exercise adaptations in skeletal muscle: benefits and pitfalls. *Biochem. Pharmacol* 147, 211–220. [PubMed: 29061342]

- Wende AR, Schaeffer PJ, Parker GJ, Zechner C, Han DH, Chen MM, Hancock CR, Lehman JJ, Huss JM, McClain DA, et al. (2007). A role for the transcriptional coactivator PGC-1alpha in muscle refueling. *J. Biol. Chem* 282, 36642–36651. [PubMed: 17932032]
- Winther AM, Bublitz M, Karlens JL, Møller JV, Hansen JB, Nissen P, and Buch-Pedersen MJ (2013). The sarcolipin-bound calcium pump stabilizes calcium sites exposed to the cytoplasm. *Nature* 495, 265–269. [PubMed: 23455424]
- Wright DC, Geiger PC, Han DH, Jones TE, and Holloszy JO (2007). Calcium induces increases in peroxisome proliferator-activated receptor gamma coactivator-1alpha and mitochondrial biogenesis by a pathway leading to p38 mitogen-activated protein kinase activation. *J. Biol. Chem* 282, 18793–18799. [PubMed: 17488713]
- Wu H, Kanatous SB, Thurmond FA, Gallardo T, Isotani E, Bassel-Duby R, and Williams RS (2002). Regulation of mitochondrial biogenesis in skeletal muscle by CaMK. *Science* 296, 349–352. [PubMed: 11951046]
- Zechner C, Lai L, Zechner JF, Geng T, Yan Z, Rumsey JW, Collia D, Chen Z, Wozniak DF, Leone TC, and Kelly DP (2010). Total skeletal muscle PGC-1 deficiency uncouples mitochondrial derangements from fiber type determination and insulin sensitivity. *Cell Metab.* 12, 633–642. [PubMed: 21109195]
- Zurlo F, Larson K, Bogardus C, and Ravussin E (1990). Skeletal muscle metabolism is a major determinant of resting energy expenditure. *J. Clin. Invest* 86, 1423–1427. [PubMed: 2243122]

Highlights

- Sarcophilin (SLN) regulates thermogenesis and energy metabolism in skeletal muscle
- Loss of SLN leads to obesity, whereas overexpression of SLN resists against obesity
- SLN promotes mitochondrial biogenesis and oxidative phenotype in glycolytic muscle
- SLN activates the CamKII-PGC1 α signaling pathway to promote mitochondrial biogenesis

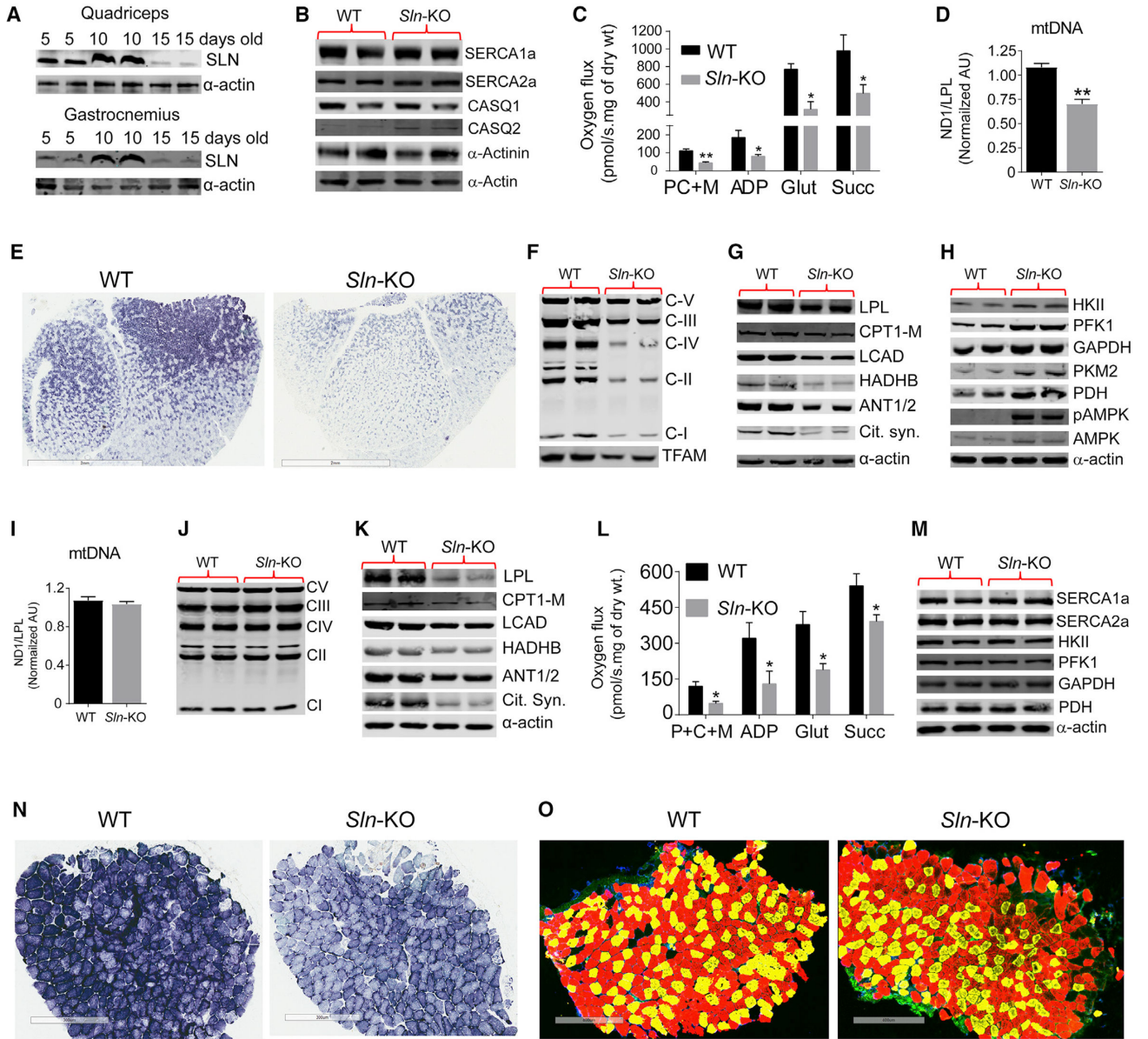


Figure 1. SLN Regulates the Mitochondrial Phenotype and Oxidative Metabolism during Neonatal Skeletal Muscle Development

(A–H) Neonatal muscle development.

(A) SLN protein expression in neonatal quadriceps and gastrocnemius of WT mice.

(B) The expression level of SERCA1a, SERCA2a, and calsequestrin 1 and 2 (CASQ1 and CASQ2) in 10-day-old WT and *Sln*-KO quadriceps muscle.

(C) Decreased fatty acid (palmitoylcarnitine) oxidation in *Sln*-KO muscle. PC, palmitoylcarnitine; M, malate; Glut, glutamate; Succ, succinate (n = 5).

(D) Decrease in mtDNA content.

(E) Succinate dehydrogenase (SDH) activity staining in 10-day-old WT and *Sln*-KO quadriceps muscle.

(F) Decreased expression of mitochondrial electron transport chain (ETC) proteins in *Sln*-KO muscle.

(G) Decreased expression of enzymes involved in fat mobilization (LPL, lipoprotein lipase), fatty acid transport (CPT1-M, carnitine palmitoyltransferase-1 mitochondrial), β -oxidation enzymes (LCAD, long-chain acyl-CoA dehydrogenase; HADHB; 3-ketoacyl-CoA thiolase, acetyl-CoA acyltransferase, or beta-ke-tothiolase), adenine nucleotide translocator (ANT), and citrate synthase.

(H) Upregulation of major glycolytic enzymes and higher levels of phosphorylated 5' adenosine monophosphate-activated protein (AMP) kinase (pAMPK) in *Sln*-KO muscle.

(I–O) Adult soleus muscle from WT and *Sln*-KO mice.

(I) mtDNA content is not altered in *Sln*-KO soleus.

(J) ETC protein expression are unchanged.

(K) *Sln*-KO soleus shows decreased expression of proteins involved in fat mobilization, fatty acid transport, β -oxidation enzymes, and citrate synthase.

(L) Decreased fatty acid oxidation in *Sln*-KO soleus muscle. P, palmitoylCoA; C, carnitine; M, malate.

(M) Levels of glycolytic enzymes are not altered.

(N) SDH activity staining of adult WT and *Sln*-KO soleus muscle.

(O) Immunostaining with myosin isoform-specific antibodies reveals that muscle fiber composition is not affected in the *Sln*-KO soleus muscle (n = 4). Yellow, myosin ATPase type I; red, myosin ATPase type IIa; green, myosin ATPase type IIb; black, myosin ATPase type x.

Data are shown as mean \pm SEM. *p < 0.01, **p < 0.001, ***p < 0.0001, t test.

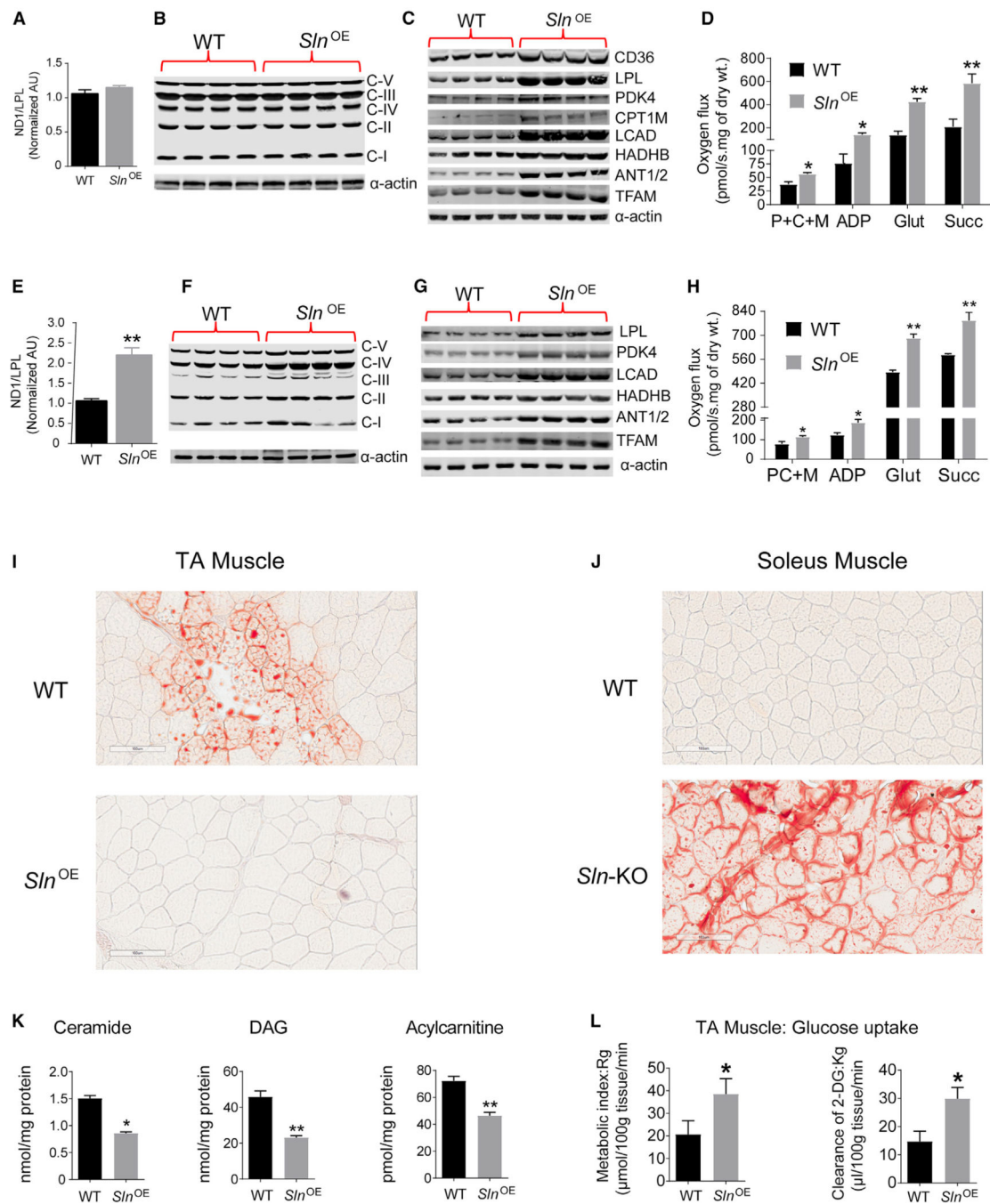


Figure 2. Transgenic Overexpression of SLN in Glycolytic Muscle (Tibialis Anterior) Programs Mitochondria to Increase Fatty Acid Metabolism and Protects from High-Fat Diet-Induced Lipotoxicity

(A–D) WT and *Sln*^{OE} mice maintained on regular chow diet.

(A) mtDNA copy number (n = 5).

(B) ETC protein expression.

(C) Expression level of fatty acid transporters (CD36 and CPT1-M), β -oxidation enzymes (LCAD and HADHB), ANT1/2, and TFAM in *Sln*^{OE} muscle is greater than in WT.

(D) Increased fatty acid oxidation in *Sln*^{OE} muscle.

- (E–L) *Sln^{OE}*, WT, and *Sln*-KO mice fed on a high-fat diet (HFD) for 12 weeks.
- (E) mtDNA copy number (n = 5).
- (F) ETC protein expression.
- (G) Regulators of oxidative metabolism.
- (H) Increased fatty acid oxidation in *Sln^{OE}* muscle oxidation (n = 5).
- (I) Oil red O staining of *Sln^{OE}* TA muscle shows no lipid accumulation.
- (J) Soleus muscle from *Sln*-KO mice showing increased lipid accumulation.
- (K) *Sln^{OE}* muscle shows lower levels of ceramides, DAG (diacylglyceride), and acylcarnitines (n = 4).
- (L) Higher rate of glucose uptake and clearance in TA muscle of *Sln^{OE}* mice (n = 5).
- Data are shown as mean ± SEM. *p < 0.01, **p < 0.001, ***p < 0.0001, t test.

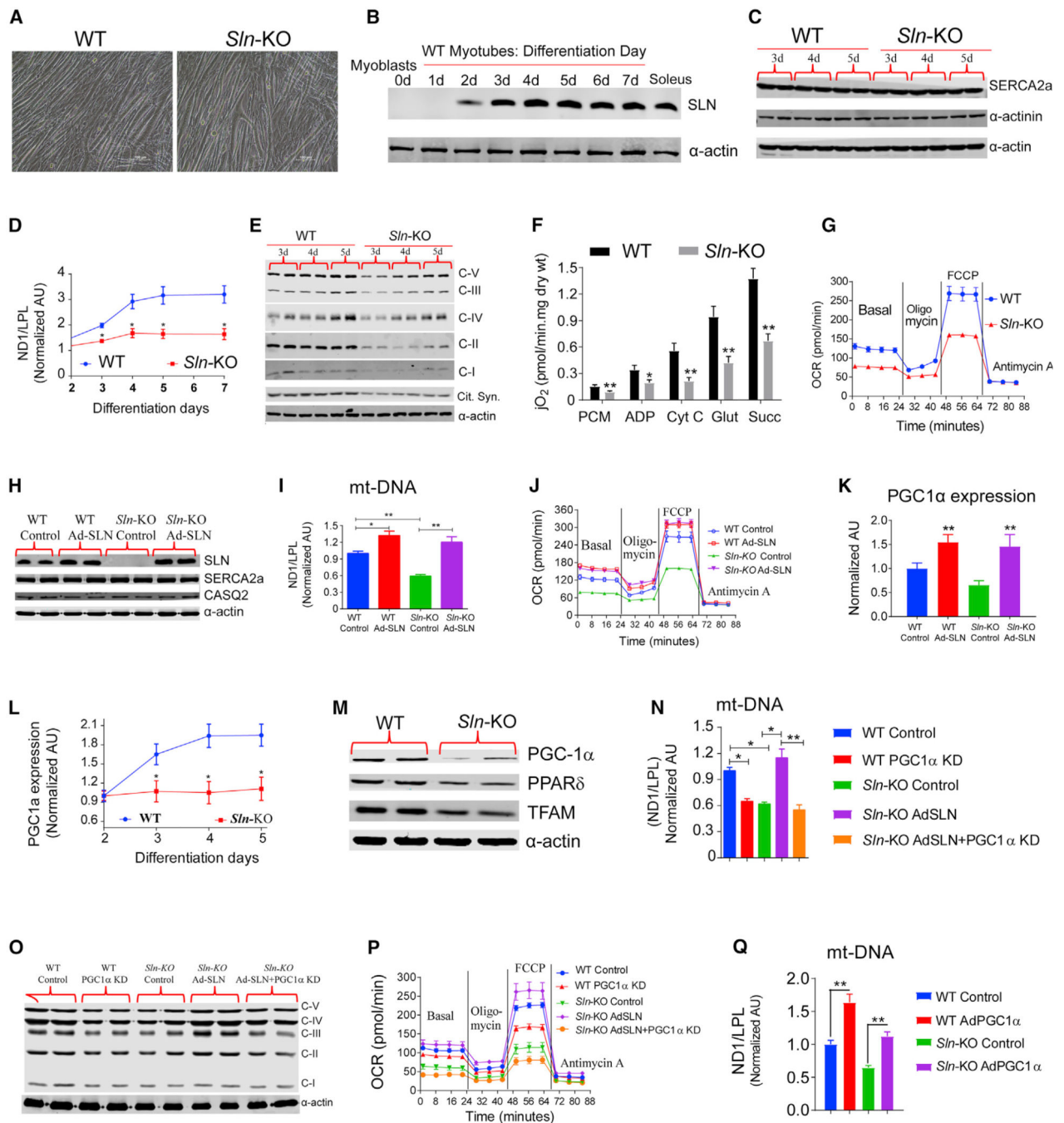


Figure 3. SLN Recruits PGC1 α to Increase Mitochondrial Biogenesis

- (A) Primary muscle myotubes derived from satellite cell culture.
- (B) Protein levels of SLN during WT primary myotube differentiation.
- (C) Expression level of SLN and SR proteins, SERCA, and CASQ in primary myotubes.
- (D) mtDNA copy number.
- (E) Mitochondrial OXPHOS protein levels during myotube differentiation.
- (F) Fatty acid-stimulated oxygen consumption in myotubes.
- (G) Oxygen consumption rate (OCR) in *Sln*-KO myotubes.

- (H–J) Adenoviral SLN gene transfer rescued muscle mitochondrial content (H and I) and OCR (J) in *Sln*-KO myotubes.
- (K) PGC1 α expression in WT and *Sln*-KO myotubes following adenoviral gene transfer.
- (L) PGC1 α gene expression during WT and *Sln*-KO myotube differentiation.
- (M) Protein expression level of PGC1 α , PPAR δ , and TFAM in myotubes.
- (N–P) mtDNA copy number (N), ETC protein expression (O), and OCR (P) following knockdown of PGC1 α and/or adenoviral SLN gene transfer in myotubes.
- (Q) Rescue of mtDNA content in *Sln*-KO myotubes by adenoviral PGC1 α gene transfection.

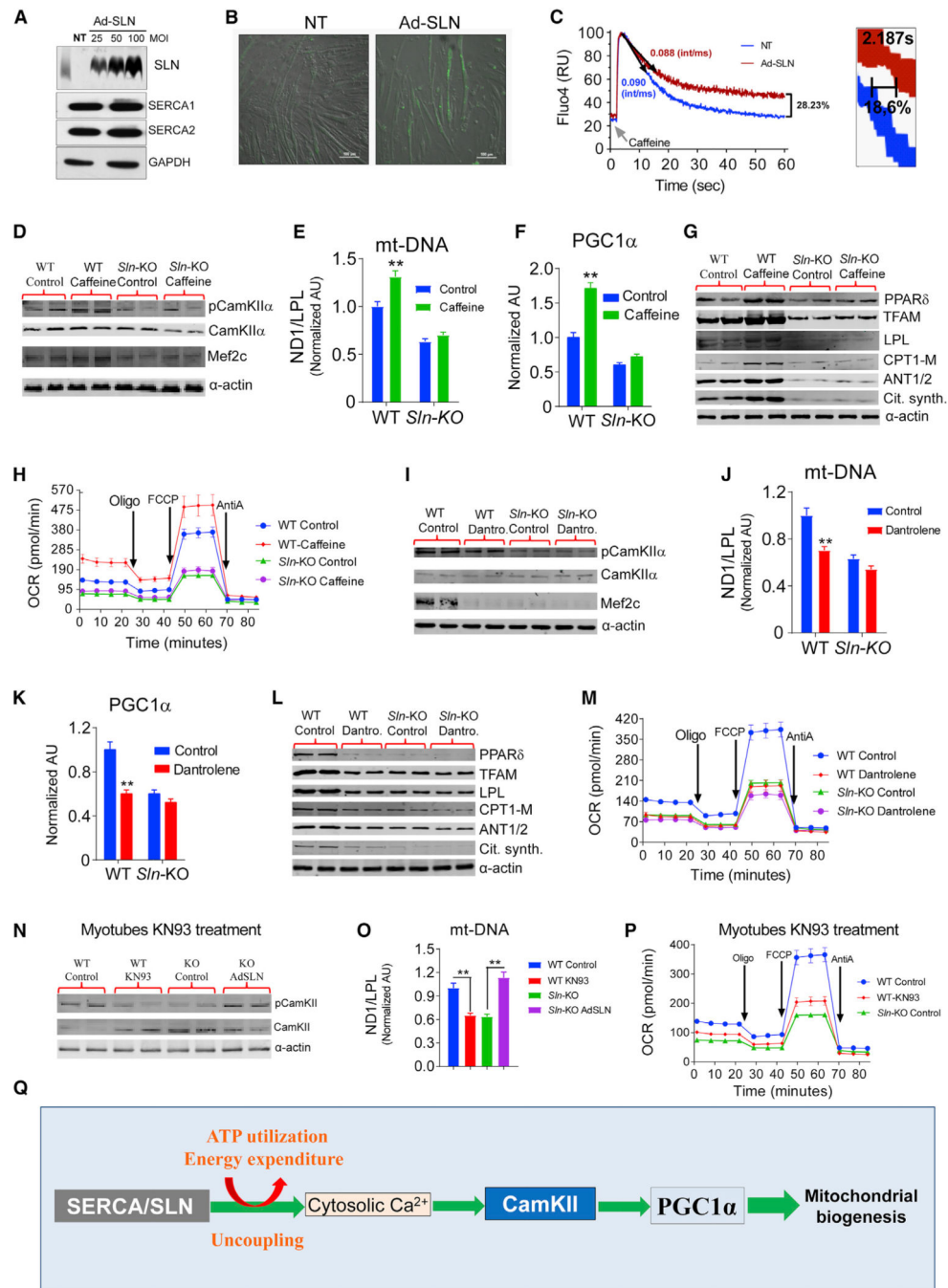


Figure 4. SLN-Mediated Increase in Mitochondrial Biogenesis Depends on SR-Ca²⁺ Cycling, Activation of CamKII, and Recruitment of the PGC1 α Axis

(A) Adenoviral-mediated expression of SLN in myotubes.
 (B) Myoplasmic Ca²⁺ as detected by Fluo-4 signal after caffeine administration.
 (C) Ca²⁺ transients after activation with caffeine, as indicated by both time measurement (in seconds) and curve slope analysis (in int/ms).
 (D) Activation of SR-Ca²⁺ cycling by caffeine treatment (3.5 mM to promote SR-Ca²⁺ release) increases CamKII phosphorylation and Mef2c expression in WT myotubes.
 (E) Increased mtDNA content.

- (F) PGC1 α expression in caffeine-treated WT myotubes.
- (G) Caffeine treatment induced expression of proteins involved in fatty acid metabolism in WT myotubes, but not in *S/n*-KO myotubes.
- (H) Caffeine increases OCR in WT myotubes.
- (I) In hibition of SR-Ca²⁺ cycling by dantrolene treatment (10 μ M to block SR-Ca²⁺ release) decreased CamKII phosphorylation and Mef2c expression.
- (J) mtDNA content.
- (K) PGC1 α expression followed by dantrolene treatment.
- (L) Dantrolene treatment decreased expression of mitochondrial transcriptional regulators and metabolic proteins.
- (M) OCR in myotubes.
- (N) Inhibition of CamKII activity by KN93 treatment (10 nM) decreased CamKII phosphorylation, whereas adenoviral SLN gene transfer in KO myotubes rescued the phosphorylation status in CamKII.
- (O and P) mtDNA content (O) and OCR (P) in myotubes following KN93 pretreatment.
- (Q) Schematic representation of how sarcolipin signals to increase mitochondrial biogenesis.